Heating effects in a chain of quantum dots

A. Glatz,[1] I. S. Beloborodov,[2] N. M. Chtchelkatchev,[1,3,4] and V. M. Vinokur[1]

[1]*Materials Science Division, Argonne National Laboratory, Argonne, Illinois 60439, USA*
[2]*Department of Physics and Astronomy, California State University Northridge, Northridge, California 91330, USA*
[3]*Institute for High Pressure Physics, Russian Academy of Sciences, Troitsk 142190, Moscow region, Russia*
[4]*L.D. Landau Institute for Theoretical Physics, Russian Academy of Sciences, 117940 Moscow, Russia*

We study heating effects in a chain of weakly coupled grains due to electron-hole pair creation. The main mechanism for the latter at low temperatures is due to inelastic electron cotunneling processes in the array. We develop a quantitative kinetic theory for these systems and calculate the array temperature profile as a function of grain parameters, bias voltage or current, and time and show that for nanoscale size grains the heating effects are pronounced and easily measurable in experiments. In the low- and high-voltage limits we solve the stationary heat-flux equation analytically. We demonstrate the overheating hysteresis in the large-current or voltage regimes. In addition we consider the influence of a substrate on the system which acts as a heat sink. We show that nanodot chains can be used as highly sensitive thermometers over a broad range of temperatures.

I. INTRODUCTION

Great efforts in contemporary materials science research focus on the understanding of thermal properties of nanoscale devices.[1–6] The electron transport through arrays of nanogranular systems is well understood[7–13] at small currents when the charge carriers have enough time to equilibrate their temperature with the temperature of the phonon bath. It is known that most of the transport characteristics of the system, e.g., the resistance, are, in fact, very sensitive to the temperature of the electronic excitations in the granules. It is much less known about *self-heating* effects in these systems when the current is not very small and the charge flow makes the internal temperature different (higher) than the temperature of the phonon bath. Understanding of the heating effects on properties of nanodevices is especially important for practical applications. In addition, recent experimental research[14–16] has focused on the application of the thermal properties of low-dimensional devices for efficient power generation. Granular thermoelectric materials have the advantage that one can control the system parameters and therefore the device properties. Due to the high sensitivity of the resistance of granular materials on temperature these materials are good candidates for broadband temperature sensors that can operate with high resolution from cryogenic up to room temperatures. This defines an urgent quest for a quantitative description of heating effects on properties of nanodevices.

In this paper we investigate the effect of inelastic cotunneling on heating of weakly coupled nanodot chain of length N coupled to two leads (see Fig. 1). We calculate the grain temperature profile as a function of grain parameters, bias current, and time for different system setups of one-dimensional chains, which may or may not be coupled to a substrate through electron-phonon collisions.

Each grain is characterized by two energy scales: (i) the mean-energy-level spacing δ and (ii) the charging energy $E_c = e^2(4\pi\kappa\epsilon_0 a)^{-1}$, where κ is the relative static permittivity of the grain material and a is the grain size. We concentrate on the case of metallic grains which are most commonly encountered in applications satisfying the inequality $E_c \gg \delta$.

In addition to the above energy scales the system under consideration is characterized by the tunneling conductances $g_t^{(i)}$. In this paper we concentrate on the regime of Coulomb blockade, meaning that the tunneling conductances are much smaller than the quantum conductance, $g_t^{(i)} \ll 1$. Our considerations are valid for temperatures $\delta < T < E_c$.

II. MECHANISM FOR GRAIN HEATING

In the considered low-temperature region, the only transport mechanism contributing to grain heating is due to inelastic cotunneling. Cotunneling allows simultaneous charge transport through several junctions by means of cooperative electron motion. Single cotunneling (Fig. 1), introduced in Ref. 17, see also the review,[18] provides a conduction channel
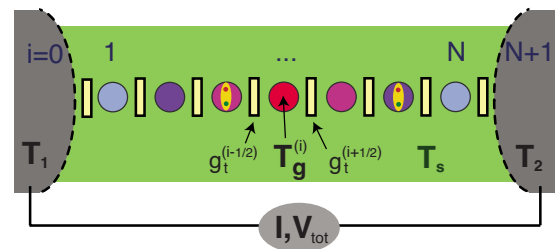

FIG. 1. (Color online) Sketch of a weakly coupled nanodot chain of length N connected to two leads with tunneling conductances $g_t^{(i\pm 1/2)} \ll 1$ (where $i \pm 1/2$ denotes the tunneling barriers right/left of grain i). The leads have the grain indices 0 and $N+1$. The lead temperatures T_1 and T_2 and substrate temperature T_s are fixed. The grain temperature $T_g^{(i)}$ depends on these temperatures and on the applied current or voltage. The main mechanism of heating in the grain due to inelastic cotunneling processes is depicted by the electron-hole pairs inside the grain which have a typical energy of $T_g^{(i)}$. The colors of the grains show a typical distribution of grain temperatures throughout the system: the coldest grains are close to the leads and the hottest in the middle of the chain.

at low applied biases, where otherwise the Coulomb blockade arising from electron-electron repulsion would suppress the current flow. The essence of a cotunneling process is that an electron tunnels via virtual states in intermediate granules thus bypassing the huge Coulomb barrier. This can be visualized as coherent superposition of two events: tunneling of the electron into a granule and the simultaneous escape of another electron from the same granule. There are two distinct mechanisms of cotunneling processes, elastic and inelastic cotunneling. Elastic cotunneling means that the electron that leaves the dot has the same energy as the incoming one. In the event of inelastic cotunneling, the electron coming out of the dot has a different energy than the entering electron. This energy difference is absorbed by an electron-hole excitation in the dot, which is left behind in the course of the inelastic cotunneling process, depicted in Fig. 1. Below we concentrate on inelastic cotunneling because only this transport mechanism contributes to heating effects. In particular, elastic cotunneling and sequential tunneling do not create electron-hole pairs in the grain.

For the quantitative description of the nonequilibrium effects leading to the heating of the chain, we consider (i) the heating due to electric resistance, (ii) the heat removal due to electron and phonon thermal conductivities, and (iii) in some cases the electron-phonon coupling of the array to a substrate. The electric conductivity and the electronic part of the thermal conductivity are governed by inelastic cotunneling processes. Using all these ingredients we can write down the kinetic equation for the grain temperatures in the following section, describing the time evolution and final temperature profile over the chain.

III. KINETIC HEAT EQUATION

For the temperatures of each grain i in the array we can write down the following kinetic equation:

$$c_v^{(i)}\frac{\partial T_g^{(i)}}{\partial t} = \sigma_{\text{in}}^{(i)}\left(\frac{V^{(i)}}{a}\right)^2 + \hat{\nabla}(\kappa^{(i)}\hat{\nabla}T_g^{(i)}) - \mathcal{P}_s^{(i)}, \quad (1)$$

where $c_v^{(i)}=(1/3)k_B^2 T_g^{(i)}\nu$ is the heat capacitance of each grain with $\nu=1/(a^3\delta)$ being the density of states in the grain; $\partial T_g^{(i)}/\partial t$ describes the change in the grain temperatures $T_g^{(i)}$ in time t. $\sigma_{\text{in}}^{(i)}$ is the cotunneling conductivity (defined below) for grain i, $V^{(i)}$ the voltage drop across grain i, $V^{(i)}=(1/2)[\phi^{(i+1)}-\phi^{(i-1)}]$, ($\phi^{(i)}$ is the electric potential of grain i); $\kappa^{(i)}$ is the thermal conductivity with $\kappa^{(i)}=\kappa_{\text{in}}^{(i)}+\kappa_{\text{ph}}^{(i)}$, where $\kappa_{\text{in}}^{(i)}$ is the electron and $\kappa_{\text{ph}}^{(i)}$ the phonon contributions to the thermal conductivity: for a single metallic grain weakly coupled to its neighbors or the leads these are given by the following expressions:[7,17,19–21]

$$\sigma_{\text{in}}^{(i)} = 2e^2 a^{-1}(g_t^{(i)})^2\frac{(k_B T_g^{(i)})^2+(eV^{(i)})^2}{\hbar E_c^2}, \quad (2a)$$

$$\kappa_{\text{in}}^{(i)} = \gamma_e a^{-1}(g_t^{(i)})^2 k_B^2 T_g^{(i)}\frac{(k_B T_g^{(i)})^2+(eV^{(i)})^2}{\hbar E_c^2}, \quad (2b)$$

$$\kappa_{\text{ph}}^{(i)} = \gamma_{\text{ph}}(\hbar l_{\text{ph}})^{-1}k_B^2 T_g^{(i)}\left(\frac{T_g^{(i)}}{\Theta_D}\right)^2. \quad (2c)$$

In Eqs. (2b) and (2c) $\gamma_{e/\text{ph}}$ are numerical coefficients ($\gamma_e=32\pi^3/15$ and $\gamma_{\text{ph}}=8\pi^2/15$, see Ref. 19), l_{ph} the phonon mean free path $l_{\text{ph}}\sim a$, and Θ_D the Debye temperature. Notice, that the temperature entering Eq. (2) is the grain temperature, $T_g^{(i)}$, which determines the number of typically involved internal-energy states of the grain. The tunneling conductances $g_t^{(i)}$ are to be understood as the averaged quantities $\sqrt{g_t^{(i-1/2)}g_t^{(i+1/2)}}$ with $i\pm 1/2$ denoting the tunneling barriers right/left of grain i. g_t is proportional to the second power of the tunneling matrix elements which is, in general, energy dependent (see discussion in Ref. 5) and therefore also temperature and voltage dependent. However, this dependence is very weak for voltage and temperature below E_c and is only relevant for second-order properties like the thermoelectric coefficient and is not taken into account here and assumed that it only depends on the morphology of the system.

The symbol $\hat{\nabla}$ in Eq. (1) is defined as an abbreviation for the central difference across the chain. In particular $\hat{\nabla}T_g^{(i)}$ stands for the *discrete* gradient of the grain temperature, i.e., $\hat{\nabla}T_g^{(i)}=[T_g^{(i+1)}-T_g^{(i-1)}]/(2a)$.

The last term in the rhs of Eq. (1), $\mathcal{P}_s^{(i)}$ describes the heat dissipation from grain i due to electron-phonon coupling of the array to a substrate and is given by[3]

$$\mathcal{P}_s^{(i)} = \Sigma_s[(T_g^{(i)})^5 - T_s^5] \quad (3)$$

with T_s being the substrate temperature and Σ_s the electron-phonon coupling constant, which is of the order 10^4 W/(m³ K⁵). This electron-phonon term is written for the *clean* case meaning that the phonon mean free path λ_{ph} is smaller than the electron mean free path, $\lambda_{\text{ph}}<l_{el}$.[22] Here, we notice that the applied current density j does not influence the substrate term.

Equation (1) has a transparent physical meaning: the energy of the electron-hole pair is released as heat, see also Fig. 1 whereas the thermal conduction to the leads removes the heat from the grain array until a steady state is reached. The typical energy of electron-hole pairs is on order of the grain temperatures, $T_g^{(i)}$, and included in the expressions for $\sigma_{\text{in}}^{(i)}$ and $\kappa_{\text{in}}^{(i)}$. The leads are assumed to be a heat sink and stay at ambient temperature T since they are much larger than the grains. The first term on the rhs of Eq. (1) describes the energy released in the grain from an electron-hole pair times the square of the discrete gradient of voltage ($V^{(i)}/a$). The latter ensures that the result is invariant under a sign change in the voltage $V^{(i)}$. The second term $\hat{\nabla}(\kappa^{(i)}\hat{\nabla}T_g^{(i)})$ describes the heat flux out of grain i. Our considerations are valid as long as the applied voltage does not breakdown the Coulomb blockade, i.e., when $eV^{(i)}<E_c$.

In typical experiments the current is kept constant and Eq. (1) can be written as

$$\hat{\nabla}(\kappa^{(i)}\hat{\nabla}T_g^{(i)}) = c_v^{(i)}\frac{\partial T_g^{(i)}}{\partial t} - \frac{(j^{(i)})^2}{\sigma_{\text{in}}^{(i)}} + \mathcal{P}_s^{(i)}, \quad (4)$$

where we introduced the current as $j^{(i)} = \sigma_{\text{in}}^{(i)}\frac{V^{(i)}}{a}$ which is constant through the whole chain. Although this equation is equivalent to Eq. (1) it has a different physical interpretation, since it describes the heat flux through the granular array. In the following we consider the case of constant current.

A. Kinetic heat equation in dimensionless units

It is convenient to rewrite the kinetic Eq. (4) in dimensionless units. Temperatures and voltages are measured in units of the first lead temperature T_1 and the time scale is in units of mean-energy-level spacing δ, i.e.,

$$\mathfrak{T}_g^{(i)} = T_g^{(i)}/T_1, \quad \mathfrak{T}_2 = T_2/T_1, \quad \mathfrak{T}_s = T_s/T_1,$$

$$\mathcal{V}^{(i)} = eV^{(i)}/(k_B T_1), \quad \tau = t\delta/\hbar, \quad (5)$$

where $\mathfrak{T}_g^{(i)}$, $\mathfrak{T}_2$, and $\mathfrak{T}_s$ are the grain, second lead, and substrate dimensionless temperatures, τ the dimensionless time, and $\mathcal{V}^{(i)}$ the dimensionless voltage drops across grain i. We also write the conductivities, Eq. (1), as

$$\sigma_{\text{in}}^{(i)} = \frac{2e^2(k_B T_1)^2}{a\hbar E_c^2}\widetilde{\sigma}_{\text{in}}^{(i)}, \quad \kappa_{\text{in}}^{(i)} = \frac{\gamma_e(k_B T_1)^3}{a\hbar E_c^2}\widetilde{\kappa}_{\text{in}}^{(i)},$$

$$\kappa_{\text{ph}}^{(i)} = \frac{\gamma_{\text{ph}}(k_B T_1)^3}{\hbar l_{\text{ph}}(\hbar\Theta_D)^2}\widetilde{\kappa}_{\text{ph}}^{(i)}, \quad (6)$$

where the "tilde" expressions are dimensionless. The dimensionless current is then $\iota^{(i)} = \widetilde{\sigma}_{\text{in}}^{(i)}\mathcal{V}^{(i)} = \frac{\hbar a^2 E_c^2}{2e(k_B T_1)^3}j^{(i)}$ and we define the dimensionless thermal conductivity as

$$\widetilde{\kappa}^{(i)} = \gamma_e\alpha\widetilde{\kappa}_{\text{in}}^{(i)} + \beta\widetilde{\kappa}_{\text{ph}}^{(i)}, \quad (7)$$

where we introduced the dimensionless parameters[23]

$$\alpha = 3\left(\frac{k_B T_1}{E_c}\right)^2, \quad \beta = 3\gamma_{\text{ph}}\frac{a}{l_{\text{ph}}}\left(\frac{T_1}{\Theta_D}\right)^2. \quad (8)$$

Substituting Eq. (6) back into Eq. (4) we obtain the following dimensionless heat equation:

$$\widetilde{\nabla}(\widetilde{\kappa}^{(i)}\widetilde{\nabla}\mathfrak{T}_g^{(i)}) = \mathfrak{T}_g^{(i)}\frac{\partial\mathfrak{T}_g^{(i)}}{\partial\tau} - 2\alpha\frac{(\iota^{(i)})^2}{\widetilde{\sigma}_{\text{in}}^{(i)}} + \mathfrak{P}_s^{(i)}, \quad (9)$$

where $\widetilde{\nabla}$ is the dimensionless central difference and the dimensionless electron-phonon coupling term to the substrate is $\mathfrak{P}_s^{(i)} = \widetilde{\Sigma}_s[(\mathfrak{T}_g^{(i)})^5 - \mathfrak{T}_s^5]$ with $\widetilde{\Sigma}_s = \frac{3\hbar a^3 T_1^3}{k_B^2}\Sigma_s$, Ref. 2. Equation (9) is the main equation which is considered in the following.

B. Discrete kinetic heat equation

Here we present the explicit expression of the kinetic heat Eq. (9) for the discrete chain of grains. First, we derive an expression for the dimensionless voltage drop on grain i, which follows from $\mathcal{V}^{(i)} = \iota^{(i)}/\widetilde{\sigma}_{\text{in}}^{(i)} = \Upsilon^{(i)}/[(\mathfrak{T}_g^{(i)})^2 + (\mathcal{V}^{(i)})^2]$ with $\Upsilon^{(i)} = \iota^{(i)}/(g_t^{(i)})^2$, leading to

$$\mathcal{V}^{(i)} = 18^{-1/3}\Xi^{(i)} - (2/3)^{1/3}(\mathfrak{T}_g^{(i)})^2/\Xi^{(i)} \quad (10)$$

with $\Xi^{(i)} = (9\Upsilon^{(i)} + \sqrt{81(\Upsilon^{(i)})^2 + 12(\mathfrak{T}_g^{(i)})^6})^{1/3}$. The total voltage drop over the chain is then $\mathcal{V}_{\text{tot}} = \Sigma_i\mathcal{V}^{(i)}$. The lhs of Eq. (9) is explicitly given by [central differences are explicitly written; cf. also Eq. (23) of Ref. 2]

$$\widetilde{\nabla}(\widetilde{\kappa}^{(i)}\widetilde{\nabla}\mathfrak{T}_g^{(i)}) = \left[\widetilde{\nabla}\widetilde{\kappa}^{(i)}\frac{\mathfrak{T}_g^{(i+1)} - \mathfrak{T}_g^{(i-1)}}{2}\right.$$

$$\left. + \widetilde{\kappa}^{(i)}(\mathfrak{T}_g^{(i+1)} + \mathfrak{T}_g^{(i-1)} - 2\mathfrak{T}_g^{(i)})\right]. \quad (11)$$

Using Eqs. (7) and (10) we obtain for the discrete gradient of thermal conductivity $\widetilde{\nabla}\widetilde{\kappa}^{(i)}$ the following expression:

$$\widetilde{\nabla}\widetilde{\kappa}^{(i)} \equiv \frac{\mathfrak{T}_g^{(i+1)} - \mathfrak{T}_g^{(i-1)}}{2}\left[\gamma_e\alpha\iota^{(i)}\frac{\partial[\mathfrak{T}_g^{(i)}/\mathcal{V}^{(i)}]}{\partial\mathfrak{T}_g^{(i)}} + 3\beta(\mathfrak{T}_g^{(i)})^2\right]. \quad (12)$$

Here we took into account the fact that the tunneling conductance $g_t^{(i)}$ is an averaged quantity for a particular grain (i) with

$$\frac{\partial[\mathfrak{T}_g^{(i)}/\mathcal{V}^{(i)}]}{\partial\mathfrak{T}_g^{(i)}} = \frac{3(\frac{3}{2})^{1/3}\Upsilon^{(i)}[12^{1/3}(\mathfrak{T}_g^{(i)})^2 + (\Xi^{(i)})^2]}{\Xi^{(i)}(\mathcal{V}^{(i)})^2\sqrt{81(\Upsilon^{(i)})^2 + 12(\mathfrak{T}_g^{(i)})^6}}, \quad (13)$$

where $\mathcal{V}^{(i)}$ is given by Eq. (10). Using Eqs. (11)–(13) we solve the kinetic heat Eq. (9) numerically for different situations. In the simulations we keep the lead temperatures $\mathfrak{T}_1 = \mathfrak{T}_g^{(0)} = 1$ and $\mathfrak{T}_2 = \mathfrak{T}_g^{(N+1)}$ fixed and integrate Eq. (9) until a steady state is reached. For the initial condition of the grain temperatures we choose a linear interpolation from $\mathfrak{T}_1$ to $\mathfrak{T}_2$.

C. Kinetic heat equation: Stationary case

Before solving kinetic heat Eq. (9) for the dimensionless temperatures $\mathfrak{T}_g^{(i)}(\tau)$ vs time τ exactly, we discuss its stationary solution corresponding to large times, $\tau \gg \tau^*$, where τ^* is some characteristic time scale which we will discuss in Sec. III E. We also consider only the case $\mathfrak{P}_s^{(i)} = 0$ (no coupling between the array and the substrate) in this section. In other words we first estimate how pronounced the effect of inelastic cotunneling on grain heating is. For large times the grain temperature reaches some constant steady-state value

$$\lim_{\tau\to\infty}\mathfrak{T}_g^{(i)}(\tau) \equiv \mathfrak{T}_g^{(i)*}, \quad (14)$$

i.e., $\partial\mathfrak{T}_g^{(i)*}/\partial\tau = 0$. In this section we consider only the stationary case and suppress the superscript $*$ in the following. Using Eq. (9) we obtain

$$\widetilde{\nabla}(\widetilde{\kappa}^{(i)}\widetilde{\nabla}\mathfrak{T}_g^{(i)}) = -2\alpha\frac{(\iota^{(i)})^2}{\widetilde{\sigma}_{\text{in}}^{(i)}}. \quad (15)$$

In the limiting cases of low voltage $(\mathcal{V}^{(i)} \ll \mathfrak{T}_g^{(i)})$ or low temperature $(\mathfrak{T}_g^{(i)} \ll \mathcal{V}^{(i)})$ one can find the analytical solution of Eq. (15) for the dimensionless grain temperature $\mathfrak{T}_g^{(i)}$. However, due to the cumbersome expression for the discrete heat flux, Eq. (11), we go over to the straight forward continuum approximation, i.e., the grain index i goes over in

coordinate x and the discrete gradients become continuum ones.

1. Low voltages

We first consider the stationary solution, Eq. (15), in the limit of small voltages, $\mathcal{V} \ll \mathfrak{T}_g$. Using Eqs. (1), (6), and (15) we obtain

$$\widetilde{\nabla}[\mathfrak{T}_g^3 \widetilde{\nabla} \mathfrak{T}_g] = -\frac{\Upsilon_L^2}{\mathfrak{T}_g^2}, \tag{16}$$

where we introduce the notation $\Upsilon_L^2 \equiv \frac{2(\iota)^2}{g_t^2(g_t^2 \gamma_e + \beta/\alpha)}$. Equation (16) can be integrated using the new variable $z(\mathfrak{T}_g) = \mathfrak{T}_g^3 \widetilde{\nabla} \mathfrak{T}_g$. Then $\widetilde{\nabla} z = z' \widetilde{\nabla} \mathfrak{T}_g = z'z/\mathfrak{T}_g^3$, where $z' = dz/d\mathfrak{T}_g$. In terms of variable z, Eq. (16) has the form

$$z'z = -\Upsilon_L^2 \mathfrak{T}_g, \tag{17}$$

leading to the solution $z = \Upsilon_L \sqrt{\mathfrak{T}_m^2 - \mathfrak{T}_g^2}$ with $\mathfrak{T}_m$ being the integration constant, physically meaning $\max_x \mathfrak{T}_g(x)$ which has the coordinate x_m, i.e., $\mathfrak{T}_m = \mathfrak{T}_g(x_m)$. Using this solution we obtain the following differential equation for the dimensionless temperature:

$$\frac{\mathfrak{T}_g^3 \nabla \mathfrak{T}_g}{\sqrt{\mathfrak{T}_m^2 - \mathfrak{T}_g^2}} = \Upsilon_L. \tag{18}$$

Integration of this equation $\int_{\mathfrak{T}_g}^{\mathfrak{T}_m} \frac{\mathfrak{T}_g^3 d\mathfrak{T}_g}{\sqrt{\mathfrak{T}_m^2 - \mathfrak{T}_g^2}} = (x_m - x)\Upsilon_L$ leads to the following solution:

$$\frac{1}{3}\sqrt{\mathfrak{T}_m^2 - \mathfrak{T}_g^2}(2\mathfrak{T}_m^2 + \mathfrak{T}_g^2) = (x_m - x)\Upsilon_L. \tag{19}$$

Introducing the new variable $y = \mathfrak{T}_g^2/\mathfrak{T}_m^2$, Eq. (19) can be written as follows:

$$y^3 + 3y^2 = 4 - (x - x_m)^2 (3\Upsilon_L/\mathfrak{T}_m^3)^2 \equiv s + 2. \tag{20}$$

The positive root of Eq. (20) reads

$$y_3 = C_{1/3}(s) - 1, \tag{21}$$

where we introduced Chebyshev's cubic root function, see Appendix

$$C_{1/3}(s) = 2 \cosh\left[\frac{1}{3}\mathrm{acosh}(s/2)\right]. \tag{22}$$

Using Eq. (21) for the dimensionless grain temperature we finally obtain

$$\frac{\mathfrak{T}_g(x)}{\mathfrak{T}_m} = \sqrt{C_{1/3}(s) - 1}, \tag{23}$$

where parameter Υ_L is defined below Eq. (16). For the symmetric case (both lead temperatures are equal, $\mathfrak{T}_1 = \mathfrak{T}_2$) Eq. (23) is plotted in Fig. 2. One can see that the maximum temperature $\mathfrak{T}_m$ is reached in the middle of the chain (Fig. 3).

2. High voltages

Here we discuss the stationary solution, Eq. (15), in the limit of small temperatures, $\mathfrak{T}_g \ll \mathcal{V}$. Using Eqs. (6) and (15) we obtain the following equation:
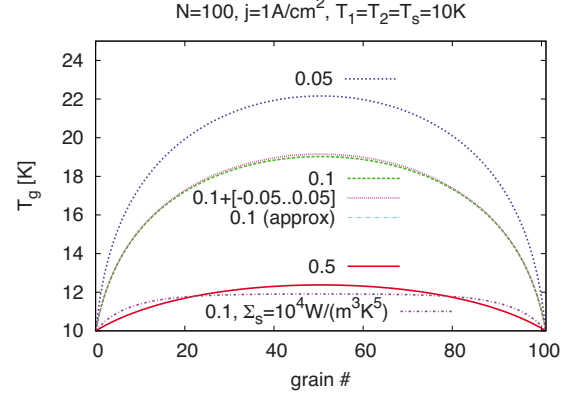

FIG. 2. (Color online) Stationary heat profiles (grain temperature T_g vs grain index) for the symmetric case where both lead temperatures coincide $T_1 = T_2 = 10$ K and for different tunneling conductances $g_t = 0.5, 0.1, 0.05$. The graph for $g_t = 0.1$ is almost identical with the profile for random $g_t^{(i)}$ with mean 0.1 and variance 0.05 (dotted, magenta) and the approximation for $g_t = 0.1$ (dashed-dotted, cyan). A curve with enabled coupling to the substrate [see definition below Eq. (9)] is shown as well for $g_t = 0.1$ and $\Sigma_s = 10^4$ W/(m^3 K^5) at a substrate temperature of $T_s = 10$ K. The current density is fixed at $j = 1$ A/cm^2 and length $N = 100$.

$$\widetilde{\nabla}[\mathfrak{T}_g \widetilde{\nabla} \mathfrak{T}_g] = -\Upsilon_H^2, \tag{24}$$

where we introduce the notation $\Upsilon_H^2 \equiv \frac{2\iota^2}{\gamma_e g_t^4 \mathcal{V}^4}$. Equation (24) can be integrated using the new variable, $z(\mathfrak{T}_g) = \mathfrak{T}_g \widetilde{\nabla} \mathfrak{T}_g$.
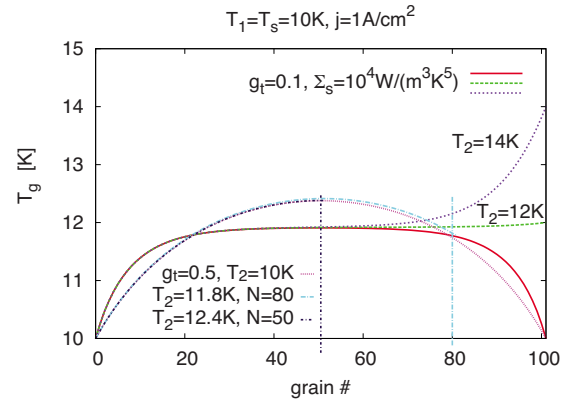

FIG. 3. (Color online) Stationary heat profiles (grain temperature T_g vs grain index) for $T_1 = T_s = 10$ K for asymmetric case with different right lead temperature T_2, in particular $T_2 > T_1$. The curves for tunneling conductance $g_t = 0.5$ for different chain lengths without substrate coupling ($\mathfrak{P}_s = 0$) are chosen in such a way that the right-lead temperature T_2 lies on the symmetric profile with $T_2 = 10$ K (number of grains $N = 100$), i.e., $T_2 = 12.4$ K for $N = 50$ and $T_2 = 11.8$ K for $N = 80$. For the latter two curves the end is marked by a vertical line since all three curves lie on top of each other. The second set of three curves is plotted for $g_t = 0.1$ and electron-phonon coupling constant $\Sigma_s = 10^4$ W/(m^3 K^5), for three different right lead temperatures $T_2 = 10, 12,$ and 14 K, written next to these curves (all for $N = 100$). The current density is fixed at $j = 1$ A/cm^2 for all graphs.
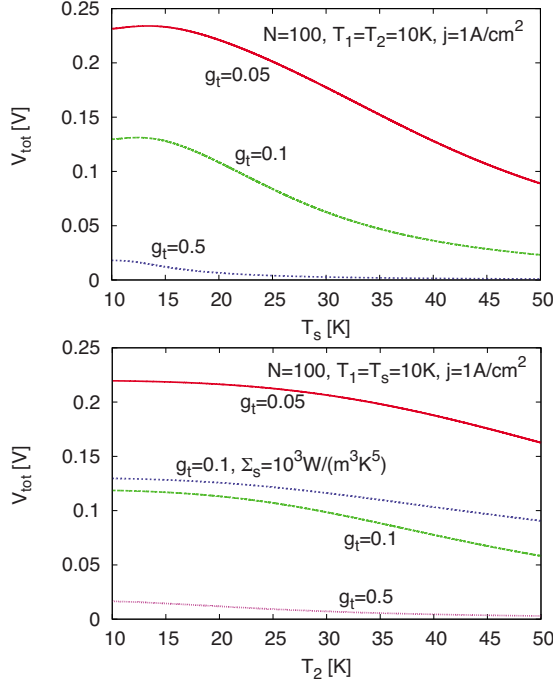
FIG. 4. (Color online) Voltage dependence of nanodot chain V_{tot} vs substrate temperature T_s (top) and right lead temperature T_2 (bottom) for different tunneling conductances g_t. All plots are for applied current density $j=1$ A/cm^2, left lead temperature $T_1=10$ K, and chain length $N=100$. In the upper panel the electron-phonon coupling constant is $\Sigma_s=10^3$ W/(m^3 K^5). In the lower plot the electron-phonon coupling is switched off, apart from the dotted blue curve marked with $g_t=0.1$, $\Sigma_s=10^3$ W/(m^3 K^5) which is coupled to a substrate at $T_s=10$ K.

Then $\widetilde{\nabla}z=z'\widetilde{\nabla}\mathfrak{T}_g=z'z/\mathfrak{T}_g$, where $z'=dz/d\mathfrak{T}_g$. In terms of variable z, Eq. (24) has the form

$$z'z=-\Upsilon_H^2\mathfrak{T}_g, \qquad (25)$$

leading to the solution $z=\Upsilon_H\sqrt{\mathfrak{T}_m^2-\mathfrak{T}_g^2}$. Equation (25) is similar to Eq. (17) obtained in the large temperature limit. The solution of Eq. (25) reads

$$\frac{\mathfrak{T}_g(x)}{\mathfrak{T}_m}=\sqrt{C_{1/3}(s)-1} \qquad (26)$$

with $s=2-(x-x_m)^2(3\Upsilon_H/\mathfrak{T}_m^3)^2$.

D. Temperature-voltage dependence

As mentioned in the introduction the chains of nanodots can be used as highly sensitive thermometers from cryogenic up to room temperature. In order to demonstrate this, we studied the total voltage drop, V_{tot}, on the chain for different substrate T_s or lead T_2 temperatures. The numerical results for V_{tot} are shown in Fig. 4 for T_s and T_2 in the range from 10 to 50 K. As one can see, the chains are particularly sensitive if the substrate (sample) is slightly above the lead temperature. It is clear that the sensitivity is reduced if only one lead is used as temperature sensor. In the case of the substrate sensor, the sensitivity range can be tuned by the tunneling

conductance of the chain. Another important issue for applications as temperature sensors is the response time of the device. In the case of the chain of grains, this response time can be reduced by (i) increasing the current density, j, (ii) having a better electron-phonon coupling to the sample, i.e., larger Σ_s, or (iii) smaller tunneling conductances, g_t; see next section. Time scales of several nanoseconds are typical for not too long chains. The length of the chain can be adjusted for best sensitivity and fastest response time. Note that the very low applied current to the system also means a low noise level in a device.

E. Kinetic heat equation: Dynamic case

In this section we estimate the characteristic dimensionless time scale τ^* [see Eq. (5)] associated with the heating of nanodot chain due to inelastic cotunneling. We define τ^* as the typical time scale to reach the maximum temperature $\mathfrak{T}_m^*$ in the chain, $\mathfrak{T}_m^*=\max_i \mathfrak{T}_g^{(i)*}=\lim_{\tau\to\infty}\mathfrak{T}_m(\tau)$. The time τ^* can be easily estimated for low voltages $\mathcal{V}\ll\mathfrak{T}$. Using the fact that for symmetric case (both leads have the same temperature, $\mathfrak{T}_1=\mathfrak{T}_2$) the maximum temperature $\mathfrak{T}_m$ is located in the middle of the chain ($i=N/2$), meaning that $\widetilde{\nabla}\mathfrak{T}_m=0$, and using Eq. (9) in the absence of a substrate, $\mathfrak{P}_s^{(i)}=0$, we obtain the following equation:

$$\mathfrak{T}_m\frac{\partial\mathfrak{T}_m}{\partial\tau}=\frac{2\alpha\iota^2}{\widetilde{\sigma}_{\text{in}}^{(N/2)}}. \qquad (27)$$

Integrating Eq. (27) for a given fixed current ι and using Eq. (6) for the dimensionless conductivity $\widetilde{\sigma}_{\text{in}}^{(N/2)}$ we obtain the following result:

$$\tau^*=\frac{g_t^2}{8\alpha\iota^2}(\mathfrak{T}_m^*)^4. \qquad (28)$$

Here the maximum temperature $\mathfrak{T}_m^*$ is implicitly defined by the following equation [see also Eq. (23)]:

$$1=\mathfrak{T}_m^*\sqrt{C_{1/3}(s)-1} \quad \text{with} \quad s=2-\frac{18(N/2)^2\iota^2}{g_t^2\left(g_t^2\gamma_e+\dfrac{\beta}{\alpha}\right)(\mathfrak{T}_m^*)^6}. \qquad (29)$$

The solution of Eq. (29), $\mathfrak{T}_m^*$ vs number of grains, N, and $\mathfrak{T}_m^*$ vs tunneling conductance, g_t, is shown in Fig. 5.

IV. OVERHEATING HYSTERESIS

If the rate of the energy supply from the external bias to the charge carriers exceeds the rate of energy losses to the environment, the phenomenon of *overheating* appears and the energy distribution function of the current carriers noticeably deviates from the equilibrium-distribution function.[24,25] One of the characteristic manifestations of the overheating effect is the onset of the "falling" region of the I-V curve where the differential conductivity $G=\partial I/\partial V<0$. The corresponding $I(V)$ characteristics is referred to as that of the S type if the current is the multivalued function of the voltage and the I-V curve of the N type corresponding to the case
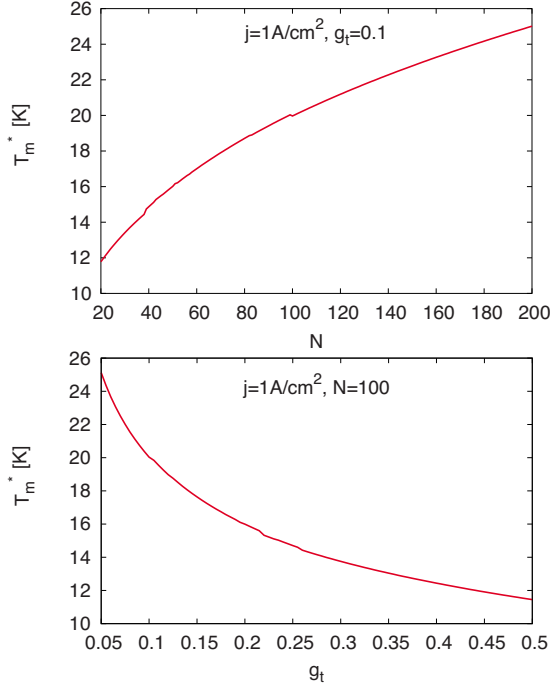
FIG. 5. (Color online) Upper panel: solution of Eq. (29) for maximum temperature $\mathfrak{T}_m^*$ vs lengths N of nanodot chain for a fixed tunneling conductance $g_t=0.1$. Low panel: $\mathfrak{T}_m^*$ vs g_t for a fixed length $N=100$. Both graphs are plotted for constant current density $j=1$ A/cm^2.

where the current is nonmonotonic but still remains a single-valued function of the voltage. The phenomenon of overheating has been a subject of the incremental interest and extensive studies during the decades, see review of Volkov and Kogan,[24] and the impressive progress in understanding of the underlying mechanisms was achieved. Recently it was suggested[26] that the mechanism of heating instability described in detail in Ref. 24 combined with the expression for the dissipated power calculated for strongly disordered conductors[27–30] (see Ref. 2 for review) can explain switching *I-V* characteristics in InO and TiN samples.

Using Eq. (9) we simulate the hysteretic overheating behavior in chains of nanograin arrays. We first increase the current from $j=0$ to 5 A/cm^2 and then decrease it back to zero. The results are shown in Fig. 6. One can see a pronounced hysteretic behavior of both the total voltage drop V_{tot} and the maximum chain temperature T_m^*. It is important to remark that this hysteretic behavior disappears for shorter chains.

V. DISCUSSIONS

In all simulations throughout this work, we use typical experimental parameters to estimate the heating effects on a chain of weakly coupled grains and presented all equations in either SI or dimensionless units. In particular, we used the following physical parameters: the grain size $a=10$ nm, Debye temperature $\Theta_D \approx 450$ K, Coulomb energy $E_c \approx 1600$ K (with relative static permittivity $\kappa=1$), mean-energy-level spacing $\delta=1$ K, phonon mean free path $l_{\text{ph}}=a$,

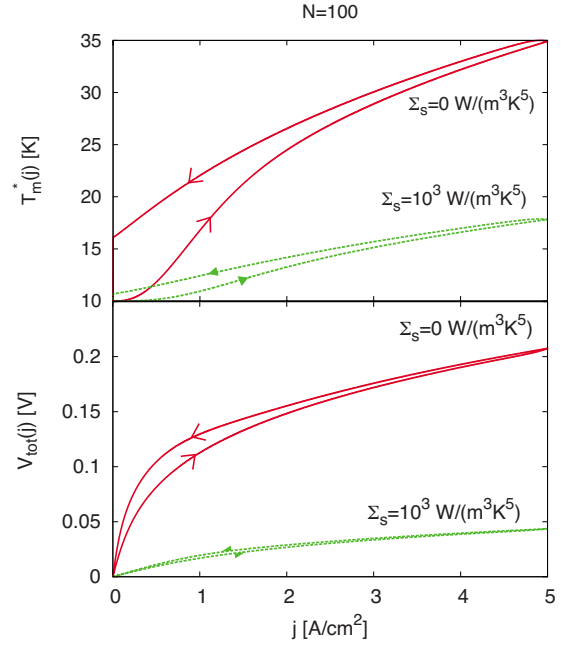FIG. 6. (Color online) Hysteretic behavior of the maximum temperature T_m^* (upper panel) and the total voltage trop V_{tot} (lower panel) vs current density j. The current density j was first increased from 0 to 5 A/cm^2 and then decreased back to 0 A/cm^2. The arrows show the direction of the hysteresis. The red curves correspond to the case with no coupling to the substrate. The green curves are shown in the presence of the substrate with electron-phonon coupling constant $\Sigma_s = 10^3$ W/(m^3 K^5). The tunneling conductance for all curves was fixed, $g_t=0.1$.

and tunneling conductance $g_t \in [0.05; 0.5]$. Furthermore we simulated typical chains of $N=100$ grains (i.e., of a few micron total length).

For the electron-phonon coupling to the substrate we used values of 10^3 or 10^4 W/(m^3 K^5) since we want to describe only the weak coupling of the chain to a different substrate. For comparison, typical values for bulk materials are much larger [on the order 10^9 W/(m^3 K^5), see, e.g., Ref. 2].

As for the analytical approximations in the low- and high-voltage regions (without substrate coupling) the particular form of the differential and later algebraic equations, allowed us to derive a closed solution using Chebyshev's cube root. As a first step we calculated the stationary heat profile of the chain under different conditions. It is important to remark that the low-voltage approximation fits very well the full simulation and randomness in the tunneling conductance has only minor effects on the final profile (provided the chain is not "broken" by a very small tunneling conductance.) Furthermore we estimated the characteristic heating time scale t^* and maximum temperature T_m^* in Eq. (28) using the analytical solution and obtained as a result $t^* \approx 0.1$ μs and $T_m^* \approx 20$ K.

These estimates can be directly compared with our simulations of Eq. (9) for rescaled maximum grain temperature $T_m(t)$ vs time t. The outcome of these simulations is shown in Fig. 7. One can see that the typical time scale t^* to reach the steady-state value T_m^* is on the order of 0.1 μs. For completeness in Fig. 7 we also presented several different curves
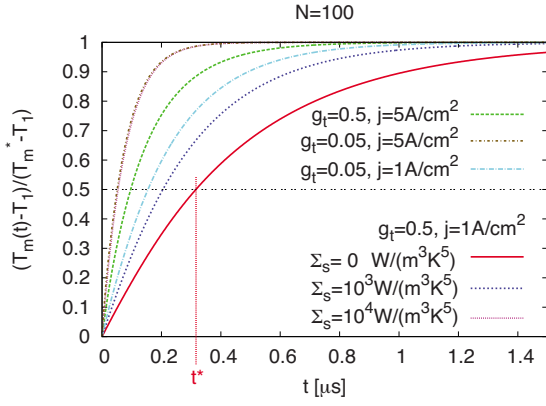
FIG. 7. (Color online) Plot of the rescaled maximum grain temperature $T_m(t)$ vs time t. The typical time scale t^* to reach the steady-state value T_m^* is shown for tunneling conductance $g_t=0.5$ and current density $j=1$ A/cm^2 (solid, red curve). For comparison also the graphs for two different substrate coupling are shown: for larger coupling the typical time scale t^* is reduced. The plot also shows the time evolution of $T_m(t)$ for different g_t and j (see legend) for zero electron-phonon coupling (no substrate): for smaller g_t or larger j, the time scale t^* can be decreased as well.

$T_m(t)$ vs time t for different tunneling conductances g_t and current densities j. In addition, we also presented two curves in the presence of the substrate: for larger coupling the typical time scale t^* is reduced. Based on the above there is a good agreement between our estimates and simulations. At this point we note that, in general, the kinetic heat Eq. (9) has an additional term proportional to the thermoelectric coefficient. Recently, thermoelectric properties of weakly coupled granular arrays were studied.[5,19] In particular, in Ref. 19 we estimated the thermoelectric and Seebeck coefficients. It was found that the thermoelectric coefficient has an additional small factor proportional to $T/E_F \ll 1$ compared to the electric and thermal conductivities, where E_F is the Fermi energy, i.e., for the temperatures under consideration this additional term in Eq. (9) would be about three orders of magnitude smaller than the others.

At this point we emphasis several aspects of our approach and approximations we used: first, the systems we discuss are characterized by two thermal equilibration times: (i) within the grain and (ii) between the grains (time scale t^* for the heating process). The relaxation time between the grain, t^*, is on the order of 10^{-7} s. The relaxation process within the grain is characterized by two scales: the typical lifetime of an electron-hole pair ($\sim 1/T_g$), which is three orders of magnitude shorter than the time scale t^* and the time scale for phonon propagation. The latter scale can be easily estimated using the fact that the phonon mean free path is on the order of the grain size and that the speed of sound in, e.g., gold is $\sim 3 \times 10^3$ m/s. As a result the typical phonon-related equilibration time scale within a metallic nanograin is on the order of 10^{-12} s. Thus, the heat distribution inside the grain happens on a much smaller time scale than time t^* and is therefore regarded as instantaneous throughout this paper.

Second, Eq. (2c) for the thermal phonon conductivity κ_{ph} is valid for temperatures below the Debye temperature, Θ_D. In addition in this temperature range κ_{ph} also depends on the
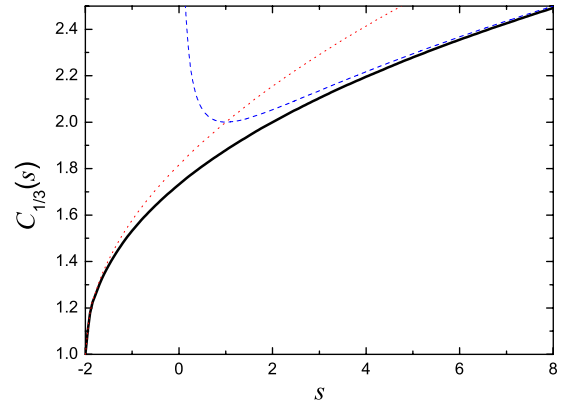

FIG. 8. (Color online) The graph of $C_{1/3}(s)$ (solid line). The graphs with the dashed and dotted lines show the behavior of the asymptotical approximations, see Eq. (A3).

dimensionality d of a sample $\kappa_{ph} \sim l_{ph}^{2-d} T[T/\Theta_D]^{d-1}$, where l_{ph} is the phonon mean free path. For phonons each grain can be considered as a three-dimensional object therefore $d=3$ and we obtain Eq. (2c). In general the phonon mean free path l_{ph} depends on temperature. However, for metallic grains of size ~ 10 nm (Fermi length $\lambda_F \sim 0.1$ nm, Debye temperature $\Theta_D \sim 500$ K) the phonon mean free path is on the order of the grain size for the temperatures under consideration and its intergrain propagation is considered to be diffusive.

Finally, in Sec. III D we state that chains of nanograins could be used as highly sensitive thermometers for cryogenic measurements. Indeed, comparing the simulated exemplary system of 100 nanoparticles to current state-of-the-art thermal diodes shows that both have a voltage sensitivity of about -5 mV/K (see Fig. 4). However, important for the sensitivity is also the noise/dissipation level in the system. In the simulations a current of 1 pA is applied, whereas in actual devices the typical operational current is several orders of magnitude larger (~ 1 μA).[31] For practical purposes it might be useful to use higher dimensional systems: nanogranular films or three-dimensional arrays which could be created through self-assembly. While these systems are highly interesting in themselves, the theoretical treatment exceeds the scope of the present work since many additional effects, e.g., percolation, have to be considered. This will be subject of a forthcoming work.

In conclusion, we have studied heating effects in one-dimensional chains of quantum dots due to inelastic electron cotunneling using a kinetic heat equation. In the low- and high-voltage limits we solved the stationary heat equation analytically. We demonstrated the possible application of chains of nanograins as highly sensitive thermometers and estimated the typical time scale to reach a steady-heat profile in these chains. Finally, we showed the overheating hysteresis in the large-current or voltage regimes. The influence of the electron-phonon coupling of the chain to a substrate was considered numerically and has pronounced effects on the stationary heat profile, the typical time scales to reach it, and the thermometric and hysteretic behavior.

APPENDIX: CUBE ROOTS

Here we discuss the positive roots of the cubic equation

$$y^3 + 3y^2 = s + 2. \tag{A1}$$

The roots of the cubic equation can be always found analytically, however, the expressions are quite cumbersome. In this paper [see Eq. (20)] we can remarkably find a simple expression for the root because Eq. (A1) reduces to the problem of finding roots of the Chebyshev polynomial. The transformation $y = \tilde{y} - 1$ reduces the left side of Eq. (A1) to the third Chebyshev polynomial, $C_3(y) = \tilde{y}^3 - 3\tilde{y}$, and the right side to s. Then the resulting equation has only one positive root

known as the Chebyshev cube root:[32] $\tilde{y} = C_{1/3}(s)$, where

$$C_{1/3}(s) = 2 \cosh\left[\frac{1}{3}\mathrm{acosh}(s/2)\right]. \tag{A2}$$

Here $\mathrm{acosh}(s/2) = \ln[(s^2 + \sqrt{s^2 - 4})/2]$ and we use the branch of the logarithm which is real on the positive real line and the branch of the square root which is positive on the real axis. Asymptotic behavior of the Chebyshev cube root is the following:

$$C_{1/3}(s) \approx \begin{cases} 1 + \sqrt{\dfrac{s+2}{3}} & \text{if } 0 < s + 2 \ll 1 \\ 2\cosh\left(\dfrac{\ln s}{3}\right) & s \gg 1. \end{cases} \tag{A3}$$

The graph of $C_{1/3}$ is shown in Fig. 8.

[1] A. Glatz and I. S. Beloborodov, Phys. Rev. B **81**, 033408 (2010).

[2] F. Giazotto, T. T. Heikkila, A. Luukanen, A. M. Savin, and J. Pekola, Rev. Mod. Phys. **78**, 217 (2006).

[3] J. P. Pekola, F. Giazotto, and O. P. Saira, Phys. Rev. Lett. **98**, 037201 (2007).

[4] I. S. Beloborodov, A. V. Lopatin, F. W. J. Hekking, R. Fazio, and V. M. Vinokur, Europhys. Lett. **69**, 435 (2005).

[5] A. Glatz and I. S. Beloborodov, Phys. Rev. B **79**, 041404(R) (2009); **79**, 235403 (2009).

[6] O.-P. Saira, M. Meschke, F. Giazotto, A. M. Savin, M. Möttönen, and J. P. Pekola, Phys. Rev. Lett. **99**, 027203 (2007).

[7] I. S. Beloborodov, A. V. Lopatin, V. M. Vinokur, and K. B. Efetov, Rev. Mod. Phys. **79**, 469 (2007).

[8] I. S. Beloborodov, K. B. Efetov, A. V. Lopatin, and V. M. Vinokur, Phys. Rev. Lett. **91**, 246801 (2003).

[9] K. B. Efetov and A. Tschersich, Europhys. Lett. **59**, 114 (2002); Phys. Rev. B **67**, 174205 (2003).

[10] M. M. Fogler, S. V. Malinin, and Th. Nattermann, Phys. Rev. Lett. **97**, 096601 (2006).

[11] I. S. Beloborodov, A. V. Lopatin, and V. M. Vinokur, Phys. Rev. B **72**, 125121 (2005).

[12] N. M. Chtchelkatchev, V. M. Vinokur, and T. I. Baturina, Phys. Rev. Lett. **103**, 247003 (2009); arXiv:1003.6105 (unpublished).

[13] Ya. I. Rodionov, I. S. Burmistrov, and N. M. Chtchelkatchev, arXiv:1003.5738 (unpublished).

[14] A. I. Boukai, Y. Bunimovich, J. Tahir-Kheli, J. K. Yu, W. A. Goddard, and J. R. Heath, Nature (London) **451**, 168 (2008).

[15] L. Shi, D. Y. Li, C. H. Yu, W. Y. Jang, D. Kim, Z. Yao, P. Kim, and A. Majumdar, J. Heat Transfer **125**, 881 (2003).

[16] E. A. Hoffmann, N. Nakpathomkun, A. I. Persson, H. Linke, H. A. Nilsson, and L. Samuelson, Appl. Phys. Lett. **91**, 252114 (2007).

[17] D. V. Averin and A. A. Odintsov, Phys. Lett. A **140**, 251 (1989).

[18] A. A. Odintsov and Y. V. Nazarov, in *Single Charge Tunneling*, edited by H. Grabert and M. H. Devoret (Plenum, New York, 1992).

[19] A. Glatz and I. S. Beloborodov, EPL **87**, 57009 (2009).

[20] L. Glazman and M. Pustilnik, in *Quantum Dots: A Doorway to Nanoscale Physics*, Lecture Notes in Physics Vol. 667, edited by W. D. Heiss (Springer, Berlin, 2005), p. 97.

[21] V. Tripathi and Y. L. Loh, Phys. Rev. Lett. **96**, 046805 (2006).

[22] For quantum dot arrays the phonon length λ_{ph} is on the order of grain size, $\lambda_{ph} \sim a$. See also discussion at the end of the paper.

[23] In typical situations the parameter β is much larger than α.

[24] A. F. Volkov and S. M. Kogan, Usp. Fiz. Nauk **96**, 633 (1968) [Sov. Phys. Usp. **11**, 881 (1969)].

[25] A. V. Gurevich and R. G. Mints, Rev. Mod. Phys. **59**, 941 (1987).

[26] M. Ovadia, B. Sacépé, and D. Shahar, Phys. Rev. Lett. **102**, 176802 (2009); D. Kalok, A. Bilusic, T. Baturina, V. Vinokur, and C. Strunk, arXiv:1004.5153 (unpublished).

[27] A. Schmid, Z. Phys. **259**, 421 (1973).

[28] M. Yu. Reizer and A. V. Sergeev, Sov. Phys. JETP **63**, 616 (1986).

[29] M. Yu. Reizer, Phys. Rev. B **40**, 5411 (1989).

[30] A. Sergeev and V. Mitin, Phys. Rev. B **61**, 6041 (2000).

[31] For comparison we used calibration data for LakeShore Cernox sensors, see, e.g., http://www.lakeshore.com/temp/sen/crtdts.html

[32] *Handbook of Mathematical Functions with Formulas, Graphs, and Mathematical Tables*, edited by M. Abramowitz and I. A. Stegun (Dover, New York, 1965), Chap. 22, p. 773.